Reconstruction of silicon surfaces: a stochastic optimization problem

Cristian V. Ciobanu[1] and Cristian Predescu[2]
[1]*Division of Engineering, Brown University, Providence, RI 02912 and*
[2]*Department of Chemistry and Kenneth S. Pitzer Center for Theoretical Chemistry, University of California, Berkeley, CA 94720*

Over the last two decades, scanning tunnelling microscopy (STM) has become one of the most important ways to investigate the structure of crystal surfaces. STM has helped achieve remarkable successes in surface science such as finding the atomic structure of Si(111) and Si(001). For high-index Si surfaces the information about the local density of states obtained by scanning does not translate directly into knowledge about the positions of atoms at the surface. A commonly accepted strategy for identifying the atomic structure is to propose several possible models and analyze their corresponding *simulated* STM images for a match with the experimental ones. However, the number of good candidates for the lowest-energy structure is very large for high-index surfaces, and heuristic approaches are not likely to cover all the relevant structural models. In this article, we take the view that finding the atomic structure of a surface is a problem of stochastic optimization, and we address it as such. We design a general technique for predicting the reconstruction of silicon surfaces with arbitrary orientation, which is based on parallel-tempering Monte Carlo simulations combined with an exponential cooling. The advantages of the method are illustrated using the Si(105) surface as example, with two main results: (a) the correct single-step rebonded structure [e.g., Fujikawa *et al.*, Phys. Rev. Lett. 88, 176101 (2002)] is obtained even when starting from the paired-dimer model [Mo *et al.*, Phys. Rev. Lett. 65, 1020 (1990)] that was assumed to be correct for many years, and (b) we have found several double-step reconstructions that have lower surface energies than any previously proposed double-step models.

PACS numbers: 68.35.Bs, 68.47.Fg, 68.18.Fg

I. INTRODUCTION

Silicon surfaces are the most intensely studied crystal surfaces since they constitute the foundation of the billion-dollar semiconductor industry. Traditionally, the low-index surfaces such as Si(001) are the widely used substrates for electronic device fabrication. With the advent of nanotechnology, the stable high-index surfaces of silicon have now become increasingly important for the fabrication of quantum devices at length scales where lithographic techniques are not applicable. Owing to their grooved or faceted morphology, some high-index surfaces can be used as templates for the growth of self-assembled nanowires. Understanding the self-organization of adatoms on these surfaces, as well as their properties as substrates for thin film growth, requires atomic-level knowledge of the surface structure. Whether the surface unit cells are small [e.g., Si(113)] or large [such as Si(5 5 12)], in general the atomic-scale models that were first proposed were subsequently contested:[1,2,3,4,5,6,7,8] the potential importance of stable Si surfaces with certain high-index orientations sparked many independent investigations, which led to different proposals in terms of surface structure.

One of the most puzzling cases has been the (105) surface, which appears on the side-facets of the pyramidal quantum dots obtained in the strained layer epitaxy of Ge or $Si_{1-x}Ge_x$ ($x > 0.2$) on Si(001). Using STM imaging, Mo and coworkers proposed the first model for this surface,[7] which was based on unrebonded monatomic steps separated by small (two-dimer wide) Si(001)-2×1 terraces. Subsequently, Khor and Das Sarma reported another possible (105) structure with a lower density of dangling bonds.[8] However, the relative surface energy of the two different reconstructions[7,8] was not computed, and the structure proposed in Ref. 8 had not, at the time, replaced the widely accepted model[7] of Mo *et al.* Only very recently it has been shown[9,10,11,12,13] that the actual (105) structure is made of single-height rebonded steps (SR), which are strongly stabilized by the compressive strains present in the Ge films deposited on Si(001)[11,12] or Si(105).[9,10,13] Other high-index surfaces such as Si(113) and Si(5 5 12) have sagas of their own,[1,2,3,4,5,6] and only in the former case there is now consensus[3] about the atomic structure.

The difficulty of finding the atomic structure of a surface is not related to the resolution of the STM techniques, or to understanding of the images obtained. After all, it is well-known that STM gives information about the local density of states at the surfaces and not necessarily about atomic coordinates.[14] A common procedure for finding the reconstructions of silicon surfaces consists in a combination of STM imaging and electronic structure calculations as follows. Starting from the bulk truncated surface and taking cues from the experimental data, one proposes several atomic models for the surface reconstructions. The proposed models are then relaxed using density-functional or tight-binding methods, and STM images are simulated in each case. At the end of the relaxation, the surface energies of the structural models are also calculated. A match with the experimental STM data is identified based on the relaxed lowest-energy structures and their simulated STM images. This proce-

dure has long become standard and has been used for many high-index orientations.[2,3,4,9,10,11,15] As described, the procedure is heuristic, since one needs to rely heavily on physical intuition when proposing good candidates for the lowest energy structures. In the case of stable high-index Si surfaces, the number of possible good candidates is rather large, and may not be exhausted heuristically; thus, worst-case scenarios in which the most stable models are not included in the set of "good candidates" are very likely. On one hand, it has been recognized[4] that the minimization of surface energy for semiconductor surfaces is not controlled solely by the reduction of the dangling bond density, but also by the amount of surface stress caused in the process. On the other hand, intuitive reasoning can tackle (at best) the problem of lowering the number of dangling bonds, but cannot account for the increase in surface stress or for the possible nanoscale faceting of certain surfaces.[16] For this reason, we adopt the view that finding the structure of high-index Si surfaces is a problem of stochastic optimization, in which the competition between the saturation of surface bonds and the increase in surface stress is intrinsically considered.

To our knowledge, a truly general and robust way of predicting the atomic structure of semiconductor surfaces –understood as finding the atomic configuration of a surface of any arbitrary crystallographic orientation without experimental input, has not been reported. It is not clear that such robust atomic-scale predictions about semiconductor surfaces can even be ventured, since theoretical efforts have been hampered by the lack of empirical or semiempirical potentials that are *both fast and transferable* for surface calculations. However, the long process which lead to the discovery of the reconstruction of the (105) surface[7,8,9,10,11,12,13] indicates a clear need for a search methodology that does not rely on human intuition. The goal of this article is to present a strategy for finding the lowest-energy reconstructions for an elemental crystal surface. While we hope that this strategy will become a useful tool for many surface scientists, the extent of its applicability remains to be explored. Our initial efforts will be focused on the surfaces of silicon because of their utmost fundamental and technological importance; nonetheless, the same strategy could be applied for any other material surfaces provided suitable models for atomic interactions are available.

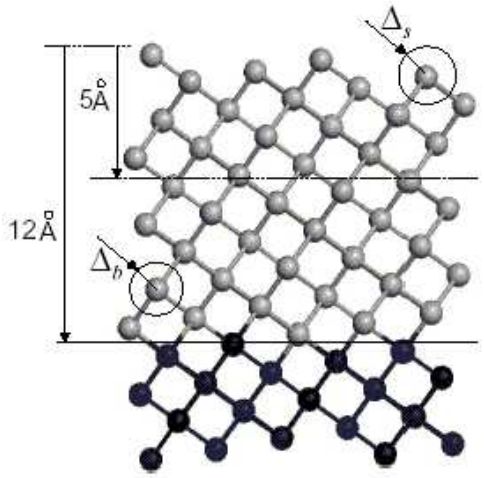

FIG. 1: Schematic computational cell: the "hot" atoms (gray) are allowed to move, while the bottom ones (black) are kept fixed at their bulk locations. Different maximum displacements Δ_s and Δ_b are allowed for the atoms that are closer to the surface and deeper in the bulk, respectively.

II. THE MONTE CARLO METHOD

A. General considerations

In choosing a methodology that can help predict the surface reconstructions, we have taken into account the following considerations. First, the number of atoms in the simulation slab is large because it includes several subsurface layers in addition to the surface ones. Moreover, the number of local minima of the potential energy surface is also large, as it scales roughly exponentially[17,18] with the number of atoms involved in the reconstruction; by itself, such scaling requires the use of fast stochastic search methods. Secondly, the calculation of interatomic forces is very expensive, so the method should be based on Monte-Carlo algorithms rather than molecular dynamics. Lastly, methods that are based on the modification of the potential energy surface (PES) (such as the basin-hoping algorithm[19]), although very powerful in predicting global minima, have been avoided as our future studies are aimed at predicting not only the correct lowest-energy reconstructions, but also the thermodynamics of the surface. These considerations prompted us to choose the parallel-tempering Monte Carlo (PTMC) algorithm[20,21] for this study. Before describing in detail the computational procedure and its advantages, we pause to discuss the computational cell and the empirical potential used.

The simulation cell has a single-face slab geometry with periodic boundary conditions applied in the plane of the surface (denoted xy), and no periodicity in the direction (z) normal to the surface (refer to Fig. 1). The "hot" atoms from the top part of the slab (corresponding to a thickness of 10–15 Å) are allowed to move, while the bottom layers of atoms are kept fixed to simulate the underlying bulk crystal. Though highly unlikely during the finite time of the simulation performed, the evaporation of atoms is prevented by using a wall of infinite energy that is parallel to the surface and situated 10 Å above it; an identical wall is placed at the level of the lowest fixed atoms to prevent the (theoretically possible) diffusion of the hot atoms through the bottom of the slab. The area of the simulation cell in the xy-plane and the number of atoms in the cell are kept fixed during each simulation; as we shall discuss in section IV, these assumptions

are not restrictive as long as we consider all the relevant values of the number of atoms per area. Under these conditions, the problem of finding the most stable reconstruction reduces to the global minimization of the total potential energy $V(\mathbf{x})$ of the atoms in the simulation cell (here $\mathbf{x}$ denotes the set of atomic positions). In order to sort through the numerous local minima of the potential $V(\mathbf{x})$, a stochastic search is necessary. The general strategy of such search (as illustrated, for example, by the simulated annealing technique[22,23]) is to sample the canonical Boltzmann distribution $\exp\left[-V(\mathbf{x})/(k_B T)\right]$ for decreasing values of the temperature T and look for the low-energy configurations that are generated.

In terms of atomic interactions, we are constrained to use empirical potentials because the highly accurate ab-initio or tight-binding methods are prohibitive. Since this work is aimed at finding the *lowest* energy reconstructions for arbitrary surfaces, the choice of the empirical potential is crucial, as different interaction models can give different energetic ordering of the possible reconstructions. Furthermore, the true structure of the surface may not even be a local minimum of the potential chosen to describe the interactions: it is the case, for example, of the adatom-interstitial reconstructions[3] of Si(113), which are not local minima of the Stillinger-Weber potential.[24] The work of Nurminen *et al.*[25] indicates that the most popular empirical potentials for silicon[24,26] are not suitable for finite-temperature simulations of surfaces. After thorough numerical experimentation with several empirical potentials, we have chosen to use the highly optimized empirical potential (HOEP) recently developed by Lenosky *et al.*[27] HOEP is fitted to a database of ab-initio calculations that includes structural and energetic information about small Si clusters, which leads to a superior transferability to the different bonding environments present at the surface.[27]

B. Advantages of the parallel tempering algorithm as a global optimizer

The parallel tempering Monte Carlo method (also known as the replica-exchange Monte-Carlo method) consists in running parallel canonical simulations of many statistically independent replicas of the system, each at a different temperature $T_1 < T_2 < \ldots < T_N$. The set of N temperatures $\{T_i,\ i = 1, 2, ...N\}$ is called a *temperature schedule*, or *schedule* for short. The probability distributions of the individual replicas are sampled with the Metropolis algorithm,[28] although any other ergodic strategy can be utilized. The key feature of the parallel tempering method is that swaps between replicas of neighboring temperatures T_i and T_j $(j = i \pm 1)$ are proposed and allowed with the conditional probability[20,21] given by

$$\min\left\{1, e^{(1/T_j - 1/T_i)[V(\mathbf{x}_j) - V(\mathbf{x}_i)]/k_B}\right\}, \qquad (1)$$

where $V(\mathbf{x}_i)$ represents the energy of the replica i and k_B is the Boltzmann constant. The conditional probability (1) ensures that the detailed balance condition is satisfied and that the equilibrium distributions are the Boltzmann ones for each temperature.

In the standard Metropolis sampling[28] of Boltzmann distributions, the probability that the Monte Carlo walker escapes from a given local minimum decreases exponentially as the temperature is lowered. In turn, the average number of Monte Carlo steps needed for the walker to escape from the trapping local minimum increases exponentially with the decrease of the temperature, a scaling that makes the search for a global minimum inefficient at low temperatures. To cope with this problem, the parallel tempering algorithm takes advantage of the fact that the Metropolis walkers running at higher temperatures have larger probabilities of jumping over energy barriers. Parallel tempering significantly decreases the time taken for the walker to escape from local minima by providing an additional mechanism for jumping between basins, namely the swapping of configurations between replicas running at neighboring temperatures. Therefore, if a given (low-temperature) replica of the system is stuck in a local minimum, the configuration swaps with walkers at higher temperatures can provide that replica with states associated with other basins (wells on the potential energy surface), ultimately driving it into the global minimum.

Because of this swapping mechanism, parallel tempering enjoys certain advantages (as a global optimizer) over the more popular simulated annealing algorithm (SA).[22,23] In order for SA to be convergent (i.e. to reach the global optimum as the temperature is lowered) the cooling schedule must be of the form[29,30]

$$T_i = \frac{T_0}{\log(i + i_0)}, \quad i \geq 1, \qquad (2)$$

where T_0 and i_0 are sufficiently large constants. Such a logarithmic schedule is too slow for practical applications, and faster schedules are routinely utilized. Common SA cooling schedules, such as the geometric or the linear ones,[22] make SA non-convergent: the Monte Carlo walker has a non-zero probability of getting trapped into minima other than the global one.

The cooling schedule implied by Eq. (2) is, of course, asymptotically valid in the limit of low temperatures. In the same limit, the PT algorithm allows for a geometric temperature schedule.[31,32] When the temperature drops to zero, the system is well approximated by a multidimensional harmonic oscillator and the acceptance probability for swaps attempted between two replicas with temperatures $T < T'$ is given by the incomplete beta function law[32]

$$Ac(T, T') \simeq \frac{2}{B(d/2, d/2)} \int_0^{1/(1+R)} \theta^{d/2-1}(1-\theta)^{d/2-1} d\theta\ , \qquad (3)$$

where d denotes the number of degrees of freedom of the system, B is the Euler beta function, and $R \equiv T'/T$.

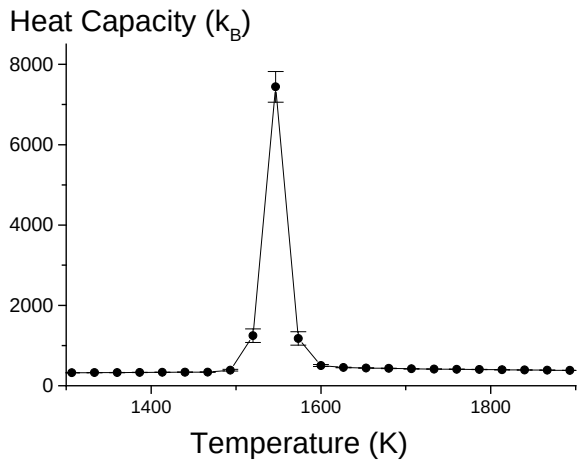

FIG. 2: Heat capacity of a Si(105) slab plotted as a function of temperature. The peak is located at 1550K; in order to avoid recalculation of the heat capacity for systems with different numbers of atoms and surface orientations, we set $T_{max} =$ 1600K as the upper limit of the temperatures range used in the PTMC simulations.

Since it depends only on the temperature ratio R, the acceptance probability (3) has the same value for any arbitrary replica running at a temperature T_i, provided that its neighboring upper temperature T_{i+1} is given by $T_{i+1} = RT_i$. The value of R is determined such that the acceptance probability given by Eq. (3) attains a prescribed value p, usually chosen greater that 0.5. Thus, the (optimal) schedule that ensures a constant probability p for swaps between neighboring temperatures is a geometric progression:

$$T_i = R^{i-1}T_{min}, \quad 1 \leq i \leq N, \tag{4}$$

where $T_{min} = T_1$ is the minimum temperature of the schedule. Though more research is required in order to better quantify the relative efficiency of the two different algorithms SA and PT, it is apparent from Eqs. (2) and (4) that the parallel tempering algorithm is a global optimizer superior to SA because it allows for a faster cooling schedule. Direct numerical comparisons of the two methods have confirmed that parallel tempering is the superior optimization technique.[33] The ideas of parallel tempering and simulated annealing are not mutually exclusive, and in fact they can be used together to design even more efficient stochastic optimizers. As shown below, such a strategy that combines parallel tempering and simulated annealing is employed for the present simulations.

C. Description of the algorithm

The typical Monte Carlo simulation done in this work consists of two main parts that are equal in terms of computational effort. In the first stage of the computation, we perform a parallel tempering run for a range of temperatures $[T_{min},\ T_{max}]$. The configurations of minimum energy are retained for each replica, and used as starting configurations for the second part of the simulation, in which each replica is cooled down exponentially until the largest temperature drops below a prescribed value. As a key feature of the procedure, the parallel tempering swaps are not turned off during the cooling stage. Thus, we are using a combination of parallel tempering and simulated annealing, rather than a simple cooling. Finally, the annealed replicas are relaxed to the nearest minima using a conjugate-gradient algorithm. We now describe in detail the stochastic minimization procedure. We shall focus, in turn, on discussing the Monte Carlo moves, the choice of the temperature range $[T_{min},\ T_{max}]$, and the total number of replicas N.

The moves of the hot atoms consist in small random displacements with the $x,\ y,\ z$ components given by

$$\Delta(2u_\alpha - 1)$$

where u_α $(\alpha = x, y, z)$ are independent random variables[34] uniformly distributed in the interval $[0, 1]$, and Δ is the maximum absolute value of the displacement. We update the positions of the individual hot atoms one at a time in a cyclic fashion. Each attempted move is accepted or rejected according to the Metropolis logic.[28] A complete cycle consisting in attempted moves for all hot particles is called a *pass* (or sweep) and constitutes the basic computational unit in this work. We have computed distinct acceptance probabilities for the hot atoms that are closer to the surface (situated within a distance of 5 Å below the surface) and for the deeper atoms, the movements of which are essentially small oscillations around the equilibrium bulk positions. Consequently, as shown in Fig. 1, we have employed two different maximal displacements, Δ_s for the surface atoms, and Δ_b for the bulk-like atoms lying in the deeper subsurface layers. The displacements Δ_s and Δ_b are tuned in the equilibration phase of the simulation in such a way that the Monte Carlo moves are accepted with a rate of 40% to 60%. This tuning of the maximal displacements has been performed automatically by dividing the equilibration phase into several blocks, computing acceptance probabilities for each block, and increasing or decreasing the size of the displacements $\Delta_{s,b}$ until the acceptance probabilities reached values between 40% and 60%. The automatization is necessary because the optimal displacements computed for replicas running at different temperatures have different values. The maximal displacement Δ_s for the surface atoms is found to be larger than the maximal displacement for the bulk-like atoms. Though expected in view of the larger mobility of the surface atoms, the difference between Δ_s and Δ_b is not substantial and the reader may safely employ a single maximal displacement for all hot atoms at a given temperature.

Parallel tempering configuration swaps are attempted between replicas running at neighboring temperatures at every 10 passes in an alternating manner, first with the

closest lower temperature then with the closest higher temperature. Exception make the two replicas that run at end temperatures $T_1 = T_{min}$ and $T_N = T_{max}$, which are involved in swaps every 20 passes. The range of temperatures $[T_{min}, T_{max}]$ and the temperature schedule $T_1 < T_2 < \cdots < T_N$ have been chosen as described below.

The maximum temperature T_{max} must be high enough to ensure that the corresponding random walker has good probability of escaping from various local minima. However, as the temperature is raised, increasingly more thermodynamic weight is placed on local minima that have high energies compared to the global minimum. Stillinger and Weber[17,18] have argued that the number of local minima increases exponentially with the dimensionality of the system. As such, the probability that the walker visits the basin of the global minimum significantly decreases with the increase of temperature. A very strong decrease occurs at the melting point, beyond which most of the configurations visited are associated with the liquid phase. The basins of these configurations are unlikely to contain the global minimum or, in fact, any of the low-energy local minima associated with meaningful surface reconstructions. Therefore, the high-temperature end must be set equal to the melting temperature.

The melting temperature of the surface slab can be determined from a separate parallel tempering simulation by identifying the peak of the heat capacity plotted as a function of temperature. As Fig. 2 shows, the melting temperature of a Si(105) sample slab with 70 hot atoms is about 1550 K. Rather than determining a melting temperature for each individual system studied, we have employed a fixed value of $T_{max} = 1600$ K. The melting temperature of the slab determined here (Fig. 2) is different from the value of 1250K reported for the bulk crystal:[27] the discrepancy is due to surface effects, finite-size effects, as well as to the fact that the hot atoms are always in contact with the rigid atoms from the bottom of the slab. Though we use $T_{max} = 1600$K for all simulations, we note that differences of 100K–200K in the melting temperature of the slab do not significantly affect the quality of the Monte Carlo sampling. For most surfaces and system sizes of practical importance, the value of 1600 K is in fact un upper bound for the melting temperature; this may sometimes cause the one or two walkers that run at the highest temperatures to be uncoupled from the rest of the simulation, since they might sample amorphous or liquid states. However, this loss in computational resources is very small compared to the additional effort that would be required by a separate determination of the heat capacity for each surface slab used.

In theory, the lowest temperature T_{min} should be set so low that the walker associated with this temperature is virtually localized in the basin associated with the global minima. Nevertheless, obstacles concerning the efficient use of computational resources prevent us from doing so. Numerical experimentation has shown that a temperature of $T_{min} = 400$ K is low enough that only local minima associated with realistic surface reconstructions are frequently visited. A further selection among these local minima is performed in the second part of the Monte Carlo simulation, when all temperatures of the initial schedule $\{T_i,\ i = 1, 2, ...N\}$ are gradually lowered to values below 100 K; as it turns out, this combination of parallel tempering and simulated annealing makes optimal use of computational resources. Below the melting point the heat capacity of the surface slab is almost constant and well approximated by the capacity of a multidimensional harmonic oscillator (refer to Fig. 2). In these conditions, the acceptance probability for swaps between neighboring temperatures T and T' is given by Eq. (3) (see also Ref. 32). It follows that the optimal temperature schedule on the interval $[T_{min}, T_{max}]$ is the geometric progression (4), where

$$R = (T_{max}/T_{min})^{1/[N(d,p)-1]}.$$

We have written $N \equiv N(d,p)$ to denote the smallest number of replicas that guarantees a swap acceptance probability of at least p for a system with d degrees of freedom. Since the best way to run PTMC calculations is to use one processor for each replica of the system, the feasibility of our simulations hinges on values of $N(d,p)$ that translate directly into available processors. The number of walkers $N(d,p)$ can be estimated[32] by

$$N(d,p) = \left[d^{1/2} \frac{\sqrt{2}\ln(T_{max}/T_{min})}{4\mathrm{erf}^{-1}(1-p)} \right] + 2, \qquad (5)$$

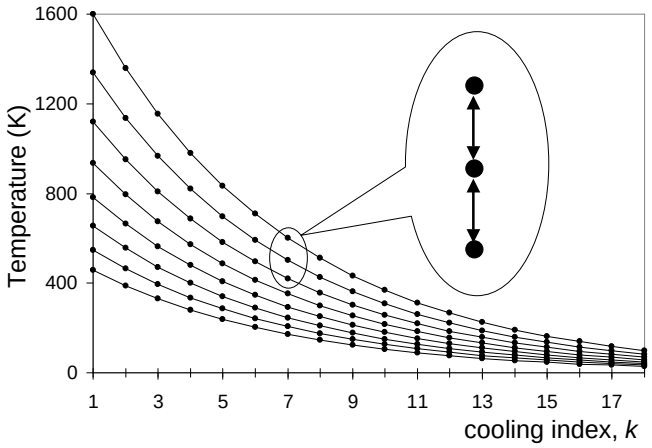

FIG. 3: Exponential cooling of the $N = 32$ Monte Carlo walkers (replicas of the surface slab) used in the simulation. For clarity, only eight walkers are shown (every fourth walker). The cooling is performed in 18 steps: at each step the temperature is modified by the same factor $\alpha = 0.85$ for all walkers, Eq. (6). For every cooling step k, we have a different parallel tempering schedule where each replica is coupled to the walkers running at neighboring temperatures via configuration swaps [Eq. (4) with $R = 4^{1/31}$]. This coupling is symbolized by the double-arrow lines in the inset.

where $[x]$ denotes the largest integer smaller than x, and erf^{-1} is the inverse error function. Based on Eq. (5), we have used $N = 32$ walkers for all simulations, which ensures a swap acceptance ratio greater than $p = 0.5$ for any system with less than 300 hot atoms, $d < 900$. The first part of all Monte Carlo simulations performed in the present article consists of a number of 36×10^4 passes for each replica, preceded by 9×10^4 passes allowed for the equilibration phase. When we retained the configurations of minimum energy, the equilibration passes have been discarded so that any memory of the starting configuration is lost.

We now describe the second part of the Monte Carlo simulation, which consists of a combination of simulated annealing and parallel tempering. At the k-th cooling step, each temperature from the initial temperature schedule $\{T_i, i = 1, 2, ..N\}$ is decreased by a factor which is independent of the index i of the replica, $T_i^{(k)} = \alpha_k T_i^{(k-1)}$. Because the parallel tempering swaps are not turned off, we require that at any cooling step k all N temperatures must be modified by the same factor α_k in order to preserve the original swap acceptance probabilities. The specific way in which α_k depends on the cooling step index k is determined by the kind of annealing being sought. In this work we have used a cooling schedule of the form

$$T_i^{(k)} = \alpha T_i^{(k-1)} = \alpha^{k-1} T_i \quad (k \geq 1), \tag{6}$$

where $T_i \equiv T_i^{(1)}$ and α is determined such that the temperature intervals $[T_1^{(k-1)}, T_N^{(k-1)}]$ and $[T_1^{(k)}, T_N^{(k)}]$ spanned by the parallel tempering schedules before and after the k-th cooling step overlap by 80%. This yields a value for α given by $(0.2T_{min} + 0.8T_{max})/T_{max} = 0.85$. We have also tested values of α larger than 0.85, and did not find any significant improvements in the quality of the sampling.

The reader may argue that the use of an exponential annealing [Eq. (6)] is not the best option for attaining the global energy minimum of the system. Apart from the theoretical considerations discussed in the preceding subsection that only a logarithmic cooling schedule would ensure convergence to the ground state,[29,30]it is known that the best annealing schedules for a given computational effort oftentimes involve several cooling-heating cycles. We emphasize that in the present simulations, the most difficult part of the sampling is taken care of by the initial PTMC run. In addition, since the configuration swaps are not turned off during cooling (refer to Fig. 3), the Monte-Carlo walkers are subjected to cooling-heating cycles through the parallel tempering algorithm.

The purpose of the annealing (second part of the simulation) is to cool down the best configurations determined by the initial parallel tempering in a way that is more robust than the mere relaxation into the nearest local minimum. If the initial PTMC run is responsible for placing the system in the correct funnels (groups of local minima separated by very large energy barriers), the annealing part of the simulation takes care of jumps between local minima separated by small barriers within a certain funnel. For this reason, the annealing is started from the configurations of minimum energy determined during the first part. The cooling is stopped when the largest temperature in the parallel tempering schedule drops below 100K. This criterion yields a total of 18 cooling steps, with 2×10^4 MC passes per replica performed at every such step.

Each cooling step is preceded by 5×10^3 equilibration passes, which are also used for the calculation of new maximal displacements Δ_s and Δ_b, as these displacements depend on temperature and must be recomputed. In fact, each cooling step is a small-scale version of the first part of the simulation. The only difference is that the cooling steps are *not* started from the configurations of minimum energy determined at the preceding cooling steps. (Otherwise, because the number of passes for a given step is quite small, the walkers might not have time to escape from some spurious local minima and we would end up restarting them over again from the respective minima.)

The third and final part of the minimization procedure is a conjugate-gradient optimization of the last configurations attained by each replica. The relaxation is necessary because we aim to classify the reconstructions in a way that does not depend on temperature, so we compute the surface energy at zero Kelvin for the relaxed slabs i, $i = 1, 2, ...N$. The surface energy γ is defined as the excess energy (with respect to the ideal bulk configuration) introduced by the presence of the surface:

$$\gamma = \frac{E_m - n_m e_b}{A} \tag{7}$$

where E_m is the potential energy of the n_m atoms that are allowed to move, $e_b = 4.6124$eV is the bulk cohesion energy given by HOEP, and A is the surface area of the slab.

III. RESULTS FOR THE SI(105) SURFACE

We have tested the method for a variety of surface orientations, such as (113), (105) and (5 5 12). In this section we are presenting results for Si(105), a choice that was determined by the ubiquity of the (105) orientation on the side facets of the pyramidal quantum dots obtained in the heteroepitaxial deposition of Ge and Si-Ge alloys on Si(001). Recent experimental and theoretical work on the atomic structure of (105) surfaces[9,10,11,12,13] provides a strong testing ground for the current investigations. In order to assess the versatility of the method and to provide a direct comparison with a previous heuristic study[13] of the (105) reconstructions, we start our PTMC simulations from each of the structures found in Ref. 13.

To establish the nomenclature for the discussion to follow, we recall that the structures were labelled by SU, SR, DU, DU1, DR, DR1, and DR2, where the first letter

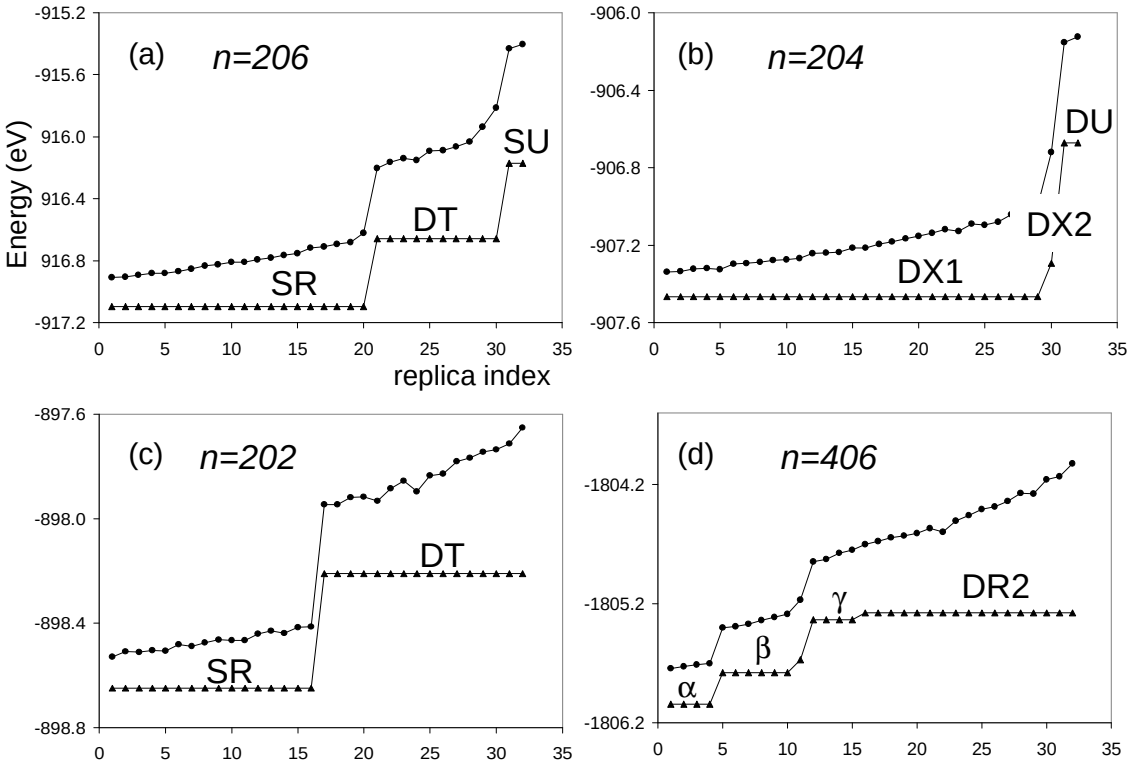

FIG. 4: Total energies of the 32 replicas of the Si(105) computational slab at the end of the cooling sequence (circles), and after the subsequent conjugate-gradient relaxation (triangles). The PTMC procedure has been started with all the replicas in the same configuration taken from the set reported in Ref. 13: SU(a), DU(b), DR(c), DR2(d). The lowest-energy configurations depend on the total number of atoms n, which is indicated in each panel. Six new double-step structural models are found, denoted by DT, DX1, DX2, DR2α, DR2β and DR2γ, with surface energies smaller than those of the corresponding starting structures

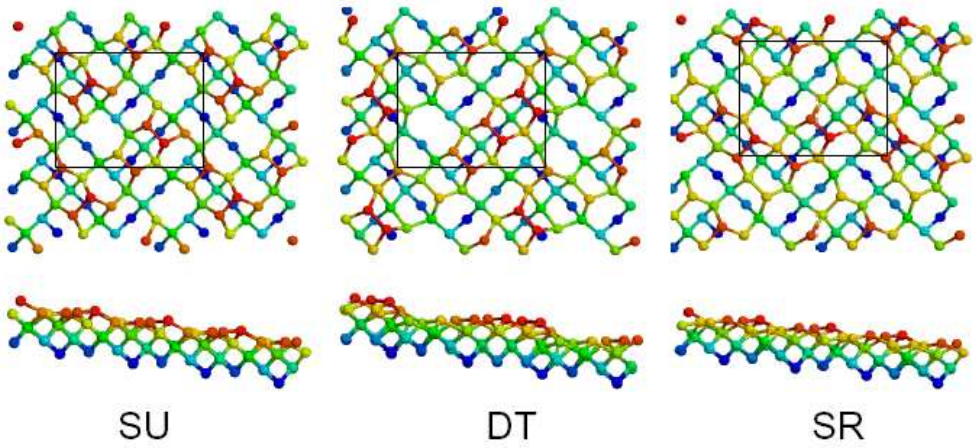

FIG. 5: Si(105) reconstructions obtained when starting from the SU model: SU, DT and SR. The DT structure is a novel double-stepped structure retrieved by replicas running at intermediate temperatures (see also Fig. 4(a)). The single-step rebonded structure[8,9,10,11,12,13] (SR) is the global optimum. The rectangle represents the surface unit cell, which is the same as the as the periodic supercell used in the simulations. Atoms are rainbow-colored according to their coordinate along the [105] direction, with the red atoms being at the highest positions.

denotes the height of the steps (single S, or double D), the second letter indicates whether the step is rebonded (R) or unrebonded (U) and the digit distinguishes between different structures that have the same broad topological features.[13] These reconstructions have different numbers of atoms and different linear dimensions of the periodic cell. The dimensions of the cell are chosen $2a \times a\sqrt{6.5}$ ($a = 5.431$Å is the bulk lattice constant of Si) for all the models considered except DR2, whose topology requires a periodic cell of $2a \times 2a\sqrt{6.5}$. The thickness of the slab corresponds to two unit cells in the z direction, with a maximum of 208 atoms, of which only about half are allowed to move.

The results of the PTMC simulations for the Si(105) surface are plotted in Fig. 4, which shows the total energy for each of the $N = 32$ replicas at the end of the cooling procedure (circles) and after the conjugate-gradient relaxation (triangles). Figs. 4(a), (b), (c) and (d) show the total energies of the reconstructions obtained starting from the SU, DU, DR and DR2 models, respectively. In each case, we have obtained at least two structures with lower surface energies than the starting configurations, which we discuss in turn.

Fig. 4(a) shows that the (starting) SU structure[7] is found only by the two replicas running at the highest temperatures, while colder walkers find a novel double-stepped structure, termed here "transitional" (DT). At even lower temperatures, the double-steps of the DT reconstruction unbunch into single-height rebonded (SR) steps; the three different configurations that correspond to the energies plotted in Fig. 4(a) are shown in Fig. 5. Therefore, the correct SR structure[9,10,11,12,13] is retrieved even when starting from the topologically different SU model. The usefulness of this PTMC simulation becomes apparent if we recall that the SU structure was widely believed to be correct for more than a decade after its publication. As we shall see, the ground state obtained in our stochastic search is independent of the initial configuration. The only condition for finding the reconstruction with the lowest surface energy is to prescribe the correct number of atoms and the correct dimensions for the simulation slab. We will address these practical aspects in the next section; for now, we continue to describe the results obtained for different numbers of atoms in the computational slab.

The simulation that starts from the DU model finds two distinct rebonded structures, denoted by DX1 and DX2 in Fig. 4(b). Both these structures are characterized by the presence of single dimers at the location of steps (see Fig. 6), which reduces the number of dangling bonds per unit area from $6db/a^2\sqrt{6.5}$ (starting structure DU) to $5db/a^2\sqrt{6.5}$. The DX1 reconstruction is the most stable, and it is obtained in all but three replicas of the system.

Although it has a small density of dangling bonds, the DR structure has large surface energy due to the $\sqrt{2} \times 1$ terrace reconstruction.[13] Since the density of dangling bonds is the lowest possible ($4db/a^2\sqrt{6.5}$), the minimization of surface energy is dictated by the reduction of surface stress. Unlike the case of SU and DU structures (described above), not a single replica have retained the starting model DR. Instead, the DT and SR structures are retrieved (refer to Fig. 4(c)). When starting from the DR2 structure we obtain at least three low energy structures denoted by DR2α, DR2β and DR2γ (Fig. 7), which have not been previously proposed in Refs. 13, 36, or elsewhere. Owing to a larger area of the slab, portions of the newly reconstructed unit cells have patches that resemble the models obtained in prior simulations. In particular, the atomic scale features of the steps on DR2α are very similar to those of the SR structure, a similarity that reflects in the very small relative surface energy of the two models (≈ 1.6meV/Å^2).

We note that the simulations described have a total number of atoms that is between $n = 202$ and $n = 206$ (Fig. 4(a) and (c)) per $2a^2\sqrt{6.5}$ area. To cover all the possibilities for intermediate numbers of atoms, we also perform a simulation with $n = 205$; this value of n does not correspond to any of the models reported in Ref. 13, and the parallel tempering run is started from a bulk-truncated configuration. In this case two new structures are found; these structures are named DY1 and DY2 and shown in Fig. 6. [The letters X and Y appearing in DX1, DX2, DY1, DY2 (all denoting double-stepped rebonded structures, Fig. 6) do not stand for particular words, they are simply intended to unambiguously label the structures in a way that does not complicate the notation.] While for the DY1 model the rebonding is realized via bridging bonds,[13] in the case of DY2 we find unexpected topological features such as fully saturated surface atoms and over-coordinated bulk atoms. Even though these structural units (seen in the DY2 panel of Fig. 6) reduce the number of dangling bonds, they also create high atomic-level stresses which make the DY2 reconstruction relatively unfavorable.

We have also performed PTMC simulations with SR, DR1 and DU1 as initial configurations, but have not obtained any other novel reconstructions. We found that SR and DR1 are the global energy minima corresponding to 206 atoms and 203 atoms, respectively. The DU1 structure[36] (202 atoms) has lead to the same reconstructions as the SU model (206 atoms). This result indicates a periodic behavior of the surface energy as a function of the total number of atoms, which will be discussed next.

IV. DISCUSSION

To further test that the lowest energy states for given number of atoms are independent of the initial configurations, we have repeated all the calculations using bulk-truncated surface slabs (Fig. 8) instead of reconstructed ones. We have varied the number of atoms n in the simulation cell between 196 and 208, where the latter corresponds to four bulk unit cells of dimensions $a\sqrt{6.5} \times a \times a\sqrt{6.5}$ stacked two by two in the [010] and [105] directions. For the cases with $n < 208$, we have

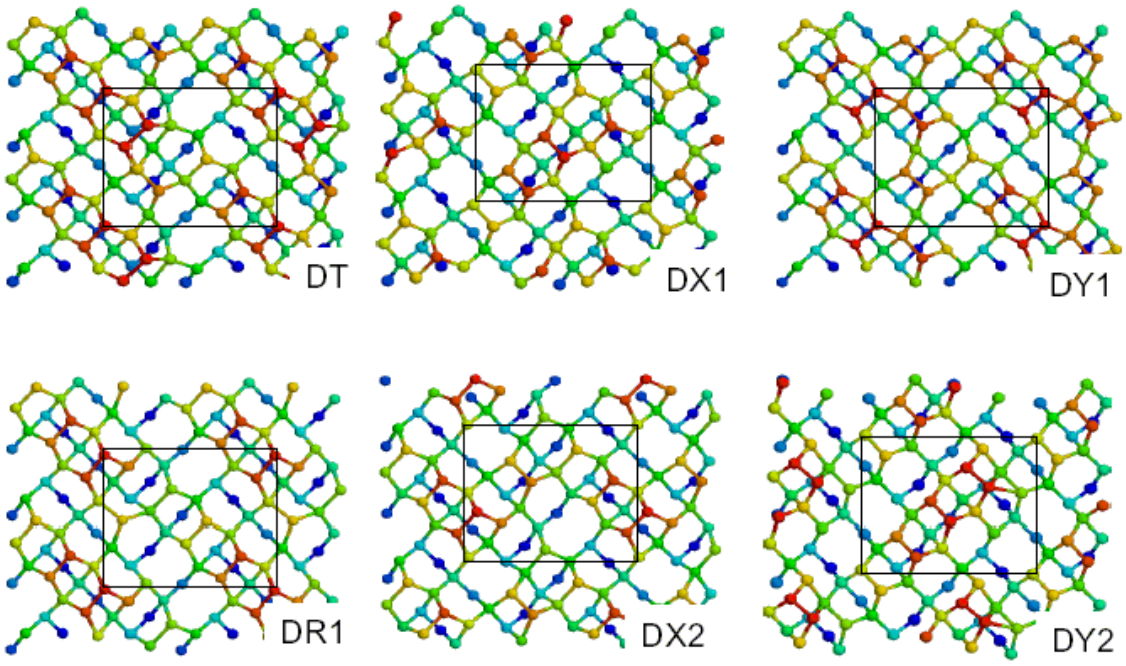

FIG. 6: Double-step reconstructions of Si(105) with periodic cells (rectangles shown) of dimensions $2a \times a\sqrt{6.5}$. The color scheme is the same as in Fig. 5. Except for DR1, all other structures are new.

started the PTMC simulations from structures obtained by taking out a prescribed number atoms from random surface sites, and have found the same ground state irrespective of the locations of the removed atoms. For values of n equal to 202, 203, 204 and 206, the ground states (global minima) are also the same as the ones obtained from the reconstructed models DR, DR1, DU, and SU, respectively. Furthermore, we have tested that even when removing arbitrary *subsurface* atoms the simulation retrieves the same ground states without increasing the computational effort. This finding speaks for the quality of the Monte Carlo sampling and gives confidence in the predictive capabilities of the method described in section II. The lowest surface energies obtained at the end of the numerical procedure are shown in Fig. 9 as a function of the number of atoms in the simulation cell. As illustrated in Fig. 9, the simulation finds the same ground states at periodic intervals of $\Delta n = 4$. At first sight, this is somewhat surprising given that the number of undercoordinated surface atoms in a bulk-truncated cell of dimensions $2a \times a\sqrt{6.5}$ is twelve (refer to Fig. 8). The reduced periodicity of the surface energy with the number of atoms in the supercell is due to the underlying crystal structure, which lowers the number of symmetry-distinct global minima to only four. Thus, we have considered all possibilities in terms of numbers of atoms in a simulation slab of area $2a^2\sqrt{6.5}$. The surface energies of the optimal reconstructions for relevant values of n, as well as those of some higher-energy structures, are collected in Table I. As shown in the table, the global minimum of the surface energy of Si(105) is obtained for the single-height rebonded structure SR. While this finding is in agreement with recent reports,[9,10,11,12,13] it is the result of an exhaustive search rather than a comparison between two[9,10,11,12] or more[13] heuristically proposed structures.

From Table I we also note that the SR and the DR2α structures have surface energies that are within 1.6meV/Å^2 from one another. This gap in the surface energy of the two models (SR and DR2) is smaller than the expected accuracy of relative surface energies determined by an empirical potential. Therefore, it is very likely that these two reconstructions can both be present on the same surface under laboratory conditions. As recently pointed out,[13] the coexistence of several configurations with different topological features but similar surface energies gives rise to the atomically rough and disordered aspect[35,36] of the Si(105) surface. The surface energies computed using HOEP for various rebonded structures (Table I) are close to the values obtained previously[13] at the tight-binding level.[37] For the unrebonded structures (SU and DU), the differences between the HOEP values and the tight-binding ones are larger: this discrepancy is caused by the inability of the HOEP interaction model to capture the tilting of the surface dimers, which is an important mechanism for the relaxation of these unrebonded configurations. Despite this shortcoming, we have found that the HOEP potential is accurate enough to predict the correct bonding topology of the global minimum reconstructions for a variety of surface orientations. If a comparison with experimental STM images is desired, further geometry optimizations are nec-

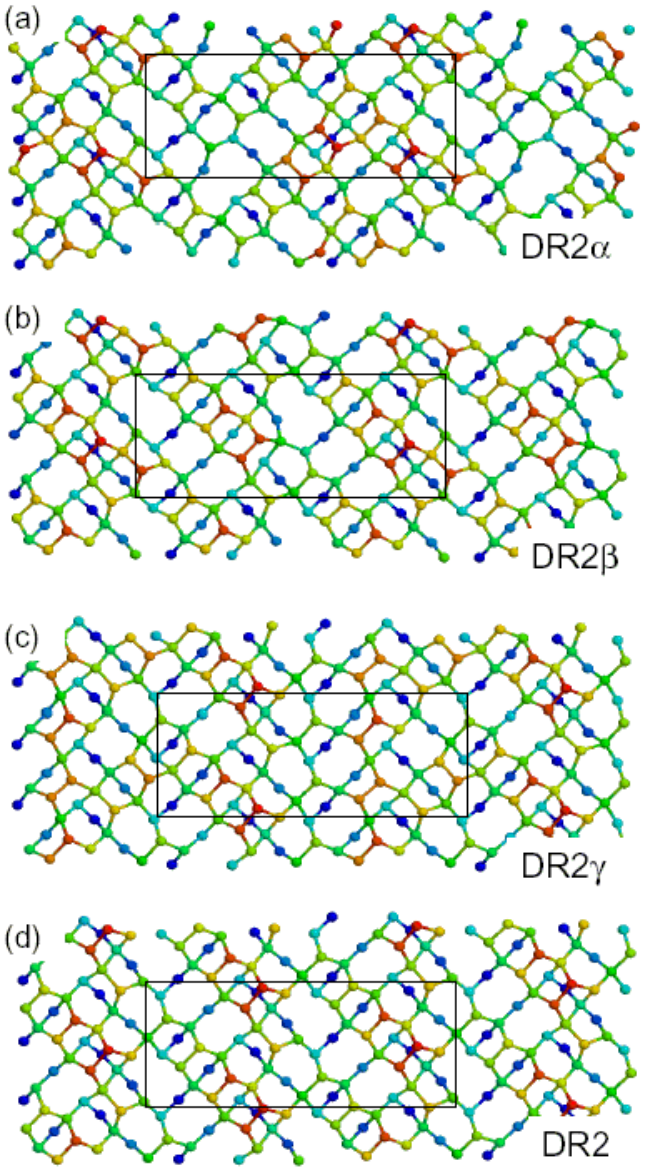

FIG. 7: Double-step reconstructions of Si(105) with periodic cells (rectangles shown) of $2a \times 2a\sqrt{6.5}$. Although the starting structure [the DR2 model[13] shown in (d)] has a reasonably low dangling bond density ($5db/a^2\sqrt{6.5}$), the Monte Carlo simulation has retrieved three more reconstructions, all having smaller surface energies (refer to Table I). These novel structures [shown in figs. (a)–(c)] are labelled by DR2α, DR2β, DR2γ. The atoms are rainbow-colored as indicated in Fig. 5.

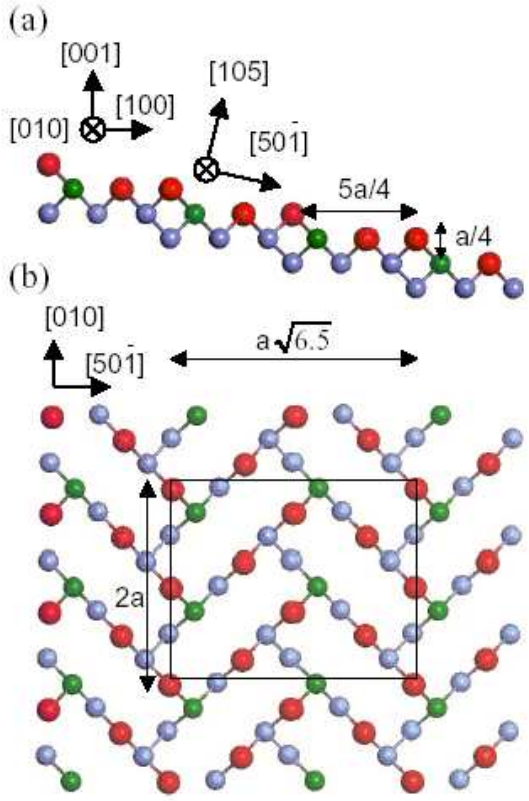

FIG. 8: Atomic structure of the bulk truncated Si(105) surface, viewed from the side (a) and from the top (b). The rectangle of dimensions $2a \times a\sqrt{6.5}$ marks the periodic cell used in most of the simulations, and contains two unit cells of the bulk-truncated surface. For clarity, only a single subsurface (001) layer is shown. In this picture (unlike in Figs. 5, 6 and 7) atoms are colored according the their number of dangling bonds (db) before reconstruction: red= $2db$, green= $1db$ and blue= $0db$.

essary at the level of electronic structure methods: these calculations would have to consider different tiltings of the surface bonds, and in each case the simulated image is to be compared with the experimental one. Thus, even for surfaces where dimer tilting is important, the Monte Carlo simulation based on the HOEP interaction model[27] can still serve as a very efficient tool to find good candidates for the lowest energy structures.

Two practical issues have to be addressed when using PTMC simulations for surface structure prediction. First consideration is related to the size of the computational cell. If a periodic surface pattern exists, the lengths and directions of the surface unit vectors can be determined accurately through experimental means (e.g., STM). In those cases, the periodic lengths of the simulation slab should simply be chosen the same as the ones found in experiments. On the other hand, when the surface does not have two-dimensional periodicity (as it is the case of unstrained Si(105) surface[35,36]), or when experimental data is not available, one should systematically test computational cells with periodic vectors that are low-integer multiples of the unit vectors of the bulk truncated surface; the latter unit vectors can be easily computed from the knowledge of crystal structure and surface orientation. Secondly, the number of atoms in the simulation cell is not *a priori* known, and there is no simple criterion to find the set of numbers that yield the lowest surface energy for a slab with arbitrary orientation. Adapting the algorithm presented in section II for

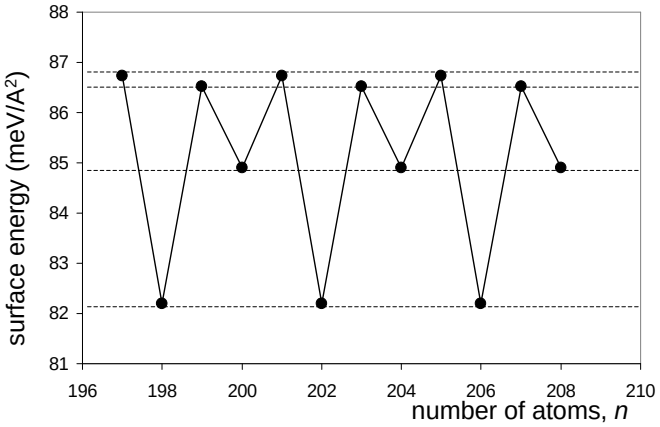

FIG. 9: Surface energy of the global minimum structure plotted versus the total number of atoms n in the simulation slab. Even though there are twelve under-coordinated atoms in each bulk-truncated periodic cell (refer to Fig. 8), the values of the surface energy repeat at intervals of $\Delta n = 4$. The underlying bulk structure reduces the number of distinct global minima to four.

n	Structure	Bond counting ($db/a^2\sqrt{6.5}$)	HOEP (meV/Å^2)	TB (meV/Å^2)
206	SR	4	82.20	82.78
	DT	4	85.12	
	SU	6	88.35	83.54
205	DY1	5	86.73	
	DY2	4.5	88.61	
204	DX1	5	84.90	
	DX2	5	86.04	
	DU	6	90.18	84.84
203	DR1	5	86.52	85.22
2×203	DR2α	4.5	83.77	
2×203	DR2β	4.5	84.64	
2×203	DR2γ	4.5	86.15	
2×203	DR2	5	86.34	83.48

TABLE I: Surface energies of different Si(105) reconstructions, calculated using the HOEP interatomic potential.[27] The structures are grouped according to the number of atoms n in the simulation cell. Atomic configurations of selected reconstructions are shown in Figs. 5, 6 and 7. The third column shows the number of dangling bonds (db) per unit area, expressed in units of $a^2\sqrt{6.5}$. The last column indicates the tight-binding[37](TB) values reported in Ref. 13.

a grand-canonical ensemble is somewhat cumbersome, as one would have to consider efficiently the combination of two different types of Monte Carlo moves: the small random displacements of the atoms (continuous) and the discrete processes of adding or removing atoms from the simulation slab. The problem of finding the correct number of atoms in the computational cell is not new, as it also appears, for example, in classic algorithms for predicting the bulk crystal structure.[38] As shown above for the case of Si(105), a successful way to deal with this problem is to simply repeat the simulation for systems with consecutive numbers of atoms, and look for a periodic behavior of the surface energy of coldest replicas as a function of the number of particles in the computational cell. Note that if the thickness of the slab is sufficiently large, such periodicity of the lowest surface energy with respect to the number of atoms in the supercell is *guaranteed* to exist: in the worst case, the periodicity will appear when an entire atomic layer has been removed from the simulation cell.

V. CONCLUDING REMARKS

In conclusion, we have developed and tested a stochastic method for predicting the atomic configuration of silicon surfaces. If suitable empirical models for atomic interactions are available, this method can be straightforwardly applied for the determination of the structure of any crystallographic surface of any other material. Using the example of Si(105), we have shown that the PTMC search is superior to heuristic approaches because it ensures that the topology corresponding to the lowest surface energy is considered in the set of good possible structural models. We have performed an exhaustive search for different numbers of atoms in the simulation cell and have found that the global minimum of the (105) surface energy is the single-height rebonded model SR, in agreement with recent studies.[9,10,11,12,13] The experiments of Zhao *et al.*[36] indicated that double-stepped structures are present on the unstrained Si(105) surface: our simulations indeed have found double-stepped models with surface energies that are close to the surface energy of the optimal SR reconstruction. In addition, these double-stepped models (termed DR2α, DR2β, and DR2γ) are energetically more favorable than the double-stepped structures proposed in Refs. 36 and 13.

We would like to comment on the key role played by the empirical potential used in the present simulations. A highly transferable interatomic potential is required for a satisfactory energetic ordering of different reconstructions. While we would not expect any empirical potential to accurately reproduce the relative surface energies of all the reconstructions found, we can at least expect that the chosen potential correctly predicts the bonding topology for well-known surface reconstructions. In this respect, the HOEP model[27] proved superior to the most widely used interatomic potentials.[24,26] Given this comparison, the results presented here would represent a validation of the work[27] towards more transferable potentials for silicon. We also hope that these results would stimulate further developments of interatomic potentials for other semiconductors.[39]

With the exception of Si(105), Si(113)[3] and (likely)

Si(114),[15] the atomic structure of other stable high-index silicon surfaces has not been elucidated, although a substantial body of STM images has accumulated to date.[40] A similar situation exists for Ge surfaces as well.[41] The methodology presented in this article can be used (either directly or in combination with the STM images[40]) to determine the configuration of all high-index Si surfaces, as long as the HOEP potential remains satisfactory for all orientations to be investigated. Furthermore, with certain modifications related to the implementation of empirical potentials for systems with *two atomic species*, the PTMC method could help bring important advances in terms of finding the thermodynamically stable intermixing composition of various nanostructures obtained by heteroepitaxial deposition of thin films on silicon substrates. Though such studies have recently been reported,[42] only the intermixing at a given atomic bonding topology has been investigated. The interplay between reconstruction and intermixing is another challenging and important problem that can be tackled via PTMC simulations. Lastly, the method presented in this article may also be used for studying the decomposition of unstable orientations into nanofacets, as well as for predicting the thermodynamics of surfaces in the presence of adsorbates or applied strain.

Acknowledgements. We gratefully acknowledge funding from National Science Foundation through the Brown MRSEC program (DMR-0079964), and Grants No. CHE-0095053 and CHE-0131114. The simulations were performed at the Center for Advanced Scientific Computation and Visualization at Brown University. We thank Professor J.D. Doll for generous support, Professor M.C. Tringides for useful discussions on the structure of high-index silicon surfaces, and Professor S.J. Singer for valuable comments on the manuscript.

[1] W. Ranke, Phys. Rev. B **41**, 5243 (1990).
[2] J. Knall, J.B. Pethica, J.D. Todd, J.H. Wilson, Phys. Rev. Lett. **66**, 1733 (1991).
[3] J.M. Dąbrowski, H.J. Müssig, G. Wolff, Phys. Rev. Lett. **73**, 1660 (1994). See also G.D. Lee, E. Yoon, Phys. Rev. B 68, 113304 (2003) and references therein.
[4] A.A. Baski, S.C. Erwin, L.J. Whitman, Science **269**, 1556 (1995).
[5] T. Suzuki, H. Minoda, Y. Tanishiro, K. Yagi, Surf. Sci. **348**, 335 (1996); *ibid.* Surf. Sci. **357-358**, 522 (1996).
[6] J. Liu, M. Takeguchi, M. Tanaka, H. Yasuda, K. Furuya, J. Electron Microsc. **50**, 541 (2001).
[7] Y.W. Mo, D.E. Savage, B.S. Swartzentruber, M.G. Lagally, Phys. Rev. Lett. **65**, 1020 (1990).
[8] K.E. Khor, S. Das Sarma, J. Vac. Sci. Technol. B **15**, 1051 (1997).
[9] Y. Fujikawa, K. Akiyama, T. Nagao, T. Sakurai, M.G. Lagally, T. Hashimoto, Y. Morikawa, K. Terakura, Phys. Rev. Lett. **88**,176101 (2002).
[10] T. Hashimoto, Y. Morikawa, Y. Fujikawa, T. Sakurai, M.G. Lagally, K. Terakura, Surf. Sci. **513**, L445 (2002).
[11] P. Raiteri, D.B. Migas, L. Miglio, A. Rastelli, H. von Känel, Phys. Rev. Lett. **88**, 256103 (2002).
[12] V.B. Shenoy, C.V. Ciobanu, L.B. Freund, Appl. Phys. Lett. **81**, 364 (2002).
[13] C.V. Ciobanu, V.B. Shenoy, C.Z. Wang, K.M. Ho, Surf. Sci. **544**, L715 (2003).
[14] H. Lüth, *Surfaces and Interfaces*, Third Edition, pp. 123-129, Springer (1995).
[15] S.C. Erwin, A.A. Baski, L.J. Whitman, Phys. Rev. Lett. **77**, 687 (1996).
[16] A.A. Baski, S.C. Erwin, L.J. Whitman, Surf. Sci. **392**, 69 (1997).
[17] F.H. Stillinger and T.A. Weber, Phys. Rev. A **28**, 2408 (1983).
[18] F.H. Stillinger, Phys. Rev. E **59**, 48 (1999).
[19] D.J. Wales and J.P.K. Doye, J. Phys. Chem. A **101**, 5111 (1997).
[20] C.J. Geyer and E.A. Thompson, J. Am. Stat. Assoc. **90**, 909 (1995).
[21] K. Hukushima and K. Nemoto, J. Phys. Soc. Jpn. **65**, 1604 (1996).
[22] S. Kirkpatrick, C.D. Gellat, M.P. Vechi, Science **220**, 671 (1983).
[23] S. Kirkpatrick, J. Stat. Phys. **34**, 975 (1984).
[24] F.H. Stillinger and T.A. Weber, Phys. Rev. B **31**, 5262 (1985).
[25] L. Nurminen, F. Tavazza, D.P. Landau, A. Kuronen, K. Kaski, Phys. Rev. B **67**, 035405 (2003).
[26] J. Tersoff, Phys. Rev. B **38**, 9902 (1988);*ibid* Phys. Rev. B **37**, 6991 (1988).
[27] T.J. Lenosky, B. Sadigh, E. Alonso, V.V. Bulatov, T. Diaz de la Rubia, J. Kim, A.F. Voter, and J.D. Kress, Modelling Simul. Mater. Sci. Eng. **8**, 825 (2000).
[28] N. Metropolis, A.W. Rosenbluth, M.N. Rosenbluth, A.M. Teller, E. Teller, J. Chem. Phys. **21**, 1087 (1953).
[29] S. Geman and D. Geman, IEEE Trans. Pattern. Anal. Machine Intelligence, **6**, 721 (1984).
[30] B. Hajek, J. Math. Oper. Res. **13**, 311 (1988).
[31] Y. Sugita, A. Kitao, and Y. Okamoto, J. Chem. Phys. **113**, 6042 (2000).
[32] C. Predescu, M. Predescu, and C.V. Ciobanu, *The incomplete beta function law for parallel tempering sampling of classical canonical systems* to appear in J. Chem Phys., preprint available at `http://www.arxiv.org/abs/physics/0310101`.
[33] J.J. Moreno, H.G. Katzgraber, A.K. Hartmann, Int. J. Mod. Phys. C **14**, 285 (2003).
[34] M. Matsumoto and T. Nishimura, in Monte Carlo and Quasi-Monte Carlo Methods 1998, edited by H. Niederreiter and J. Spanier (Springer-Verlag, New York, 2000), pp. 56–69. We used the random number generator library downloaded from `http://www.math.keio.ac.jp/~matumoto/emt.html`.
[35] M. Tomitori, K. Watanabe, M. Kobayashi, F. Iwawaki, O. Nishikawa, Surf. Sci. **301**, 214 (1994).
[36] R.G. Zhao, Z. Gai, W. Li, J. Jiang, Y. Fujikawa, T. Sakurai, W.S. Yang, Surf. Sci. **517**, 98 (2002).
[37] C.Z. Wang, B.C. Pan, K.M. Ho, J. Phys.: Condens. Matter **11**, 2043 (1999).

[38] M. Parrinello and A. Rahman, J. Appl. Phys. **52**, 7182 (1981).
[39] Research is currently underway for the development of HOEP-type potentials for pure carbon and Si-C mixtures (Fei Gao, private communication).
[40] Z. Gai, R.G. Gao, W. Li, Y. Fujikawa, T. Sakurai, W.S. Yang, Phys. Rev. B **64**, 125201 (2001).
[41] Z. Gai, X. Li, R.G. Gao, W.S. Yang, Phys. Rev. B **57**, R15060 (1998).
[42] L. Nurminen, F. Tavazza, D.P. Landau, A. Kuronen, and K. Kaski Phys. Rev. B **68**, 085326 (2003).